JACS
JOURNAL OF THE AMERICAN CHEMICAL SOCIETY

pubs.acs.org/JACS

Article

Inverted Binding of Non-natural Substrates in Strictosidine Synthase Leads to a Switch of Stereochemical Outcome in Enzyme-Catalyzed Pictet–Spengler Reactions

Elisabeth Eger, Adam Simon, Mahima Sharma, Song Yang, Willem B. Breukelaar, Gideon Grogan,* K. N. Houk,* and Wolfgang Kroutil*

Cite This: *J. Am. Chem. Soc.* 2020, 142, 792–800

Read Online

ACCESS | Metrics & More | Article Recommendations | Supporting Information

ABSTRACT: The Pictet–Spengler reaction is a valuable route to 1,2,3,4-tetrahydro-β-carboline (THBC) and isoquinoline scaffolds found in many important pharmaceuticals. Strictosidine synthase (STR) catalyzes the Pictet–Spengler condensation of tryptamine and the aldehyde secologanin to give (*S*)-strictosidine as a key intermediate in indole alkaloid biosynthesis. STRs also accept short-chain aliphatic aldehydes to give enantioenriched alkaloid products with up to 99% ee STRs are thus valuable asymmetric organocatalysts for applications in organic synthesis. The STR catalysis of reactions of small aldehydes gives an unexpected switch in stereopreference, leading to formation of the (*R*)-products. Here we report a rationale for the formation of the (*R*)-configured products by the STR enzyme from *Ophiorrhiza pumila* (*Op*STR) using a combination of X-ray crystallography, mutational, and molecular dynamics (MD) studies. We discovered that short-chain aldehydes bind in an inverted fashion compared to secologanin leading to the inverted stereopreference for the observed (*R*)-product in those cases. The study demonstrates that the same catalyst can have two different productive binding modes for one substrate but give different absolute configuration of the products by binding the aldehyde substrate differently. These results will guide future engineering of STRs and related enzymes for biocatalytic applications.

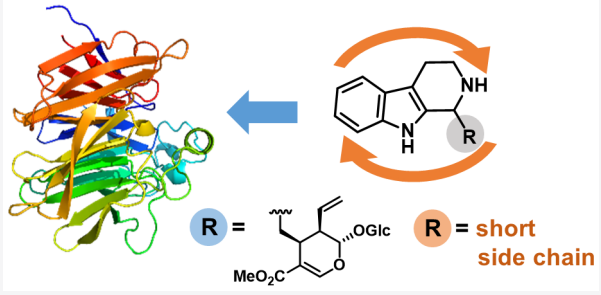

INTRODUCTION

Isoquinoline and β-carboline derivatives are both widespread structural motifs found in alkaloids isolated from various plants and animals. The isoquinoline scaffold is a building block of many pharmaceutically important drugs such as the antispasmodic papaverine and the analgesic codeine.[1] β-Carboline alkaloids exhibit a wide range of psychopharmacological effects through inhibition of monoamine oxidases or by binding to benzodiazepine receptors.[2]

The Pictet–Spengler reaction, by which 1,2,3,4-tetrahydro-β-carbolines (THBCs) and isoquinolines are synthesized from amines and aldehydes, represents an important synthetic procedure for the preparation of alkaloid derivatives and pharmaceuticals since its discovery more than a century ago.[3] The development of asymmetric synthetic versions of the reaction has sparked great interest. In addition to diastereoselective approaches, where stereocontrol can be exerted by either the amine[4] or the carbonyl substrate,[5] using a chiral auxiliary,[6] several procedures employing chiral catalysts, such as Bronsted acids,[7] Lewis acids,[8] or thiourea compounds,[9] have also been described in literature.

In nature, the equivalent reaction is catalyzed by enzymes known as "Pictet–Spenglerases" (PSases). Since the identification of the first PSase in 1976[10] this enzyme family has been constantly growing. In addition to the well-investigated representatives norcoclaurine synthase (NCS)[11] and strictosidine synthase (STR), many PSases, such as deacetylipecoside synthase (DIS) and deacetylisoipecoside synthase (DIIS) from *Alangium lamarckii*,[12] SfmC-C from *Streptomyces lavendulae*,[13] McbB from *Marinactinospora thermotolerans*,[14] and NscbB (from *Nocardiopsis synnemataformans* DSM 44143),[15] have been identified; however, structural, mechanistic, or biosynthetic applications of the latter have not been intensively studied.

The first identified representative of "Pictet–Spenglerases", STR from *Rauvolfia serpentina* (*Rs*STR, EC 4.3.3.2), catalyzes the stereoselective condensation of tryptamine (**1**) and secologanin, leading to the formation of (*S*)-strictosidine, a central intermediate in the biosynthetic pathway of indole alkaloids (Scheme 1A).[16] Crystal structures of *Rs*STR and mechanistic studies revealed that the reaction is catalyzed by a glutamate residue, Glu309, in the active site pocket, likely

Received: August 12, 2019
Published: January 7, 2020

https://dx.doi.org/10.1021/jacs.9b08704
J. Am. Chem. Soc. 2020, 142, 792–800

Scheme 1. Reactions Catalyzed by Strictosidine Synthase (STR)[b]

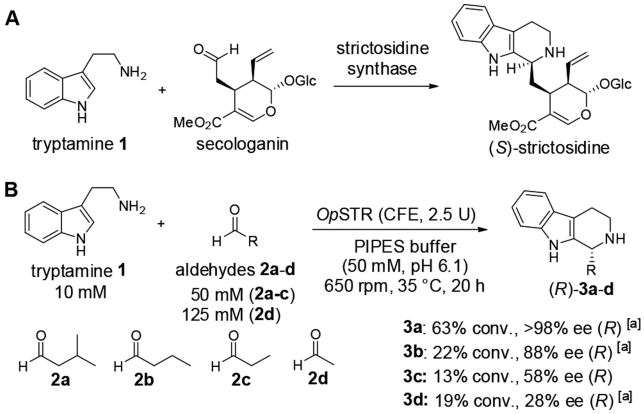

[a]Results published previously.[20b] [b]A: natural reaction of tryptamine with secologanin yielding (*S*)-strictosidine; B: reactions between tryptamine and small aliphatic aldehydes **2a–d** resulted in the formation of the corresponding (*R*)-configured tetrahydro-*β*-carbolines **3**.

assisted by neighboring tyrosine and histidine.[17] Evaluation of the synthetic potential of this and other STRs revealed a relatively broad applicability of various tryptamine analogues as substrates.[17c,18] In addition to secologanin analogues,[18c,19] selected aldehydes bearing shorter side chains were accepted by the enzyme, although with lower activities.[20] However, interestingly, we discovered that for small aliphatic aldehydes (e.g., **2a–d**) the corresponding (*R*)-configured THBC products were obtained employing, for example, the STR from *Ophiorrhiza pumila* (*Op*STR) or *Rs*STR with an ee of >98% for **3a** (Scheme 1B), in contrast to the absolute configuration of the natural (*S*)-configured product (*S*)-strictosidine.[20b]

We have now investigated the origin of this switch in stereopreference from (*S*) for the natural reaction (tryptamine with secologanin) to (*R*) when using non-native aldehydes **2a–d** as substrates with tryptamine employing the STR from *Ophiorrhiza pumila* (*Op*STR). We use X-ray crystallography, mutational analysis, and MD simulations to determine the origin of this unexpected phenomenon.

RESULTS AND DISCUSSION

In a first attempt to elucidate the origin of the (*R*)-stereoselectivity of *Op*STR with aldehydes **2b–d** (Scheme 1B), X-ray crystallographic studies were performed with *Op*STR cocrystallized with racemic THBC products **3a–c** as ligands. The overall architecture of *Op*STR is a six-bladed *β*-propeller fold (Figure 1), as previously observed in crystal structures of related enzymes such as *Rs*STR. Here each blade consists of a four-stranded antiparallel *β*-sheet arranged around a central axis. The individual strands are twisted, resulting in an almost perpendicular orientation of the fourth strand to the first inner strand. One of these *β*-sheets (*β*-sheet 1, Figure 1) is formed from one strand from the N-terminus and three strands from the C-terminus, forming the so-called "velcro closure" present in most *β*-propeller proteins. Additionally, four short *α*-helices located at the outer surface of the propeller are present in the structure of *Op*STR. One of these helices situated on top of the central axis of the enzyme forms the entrance to the active site pocket. Two of these helices are

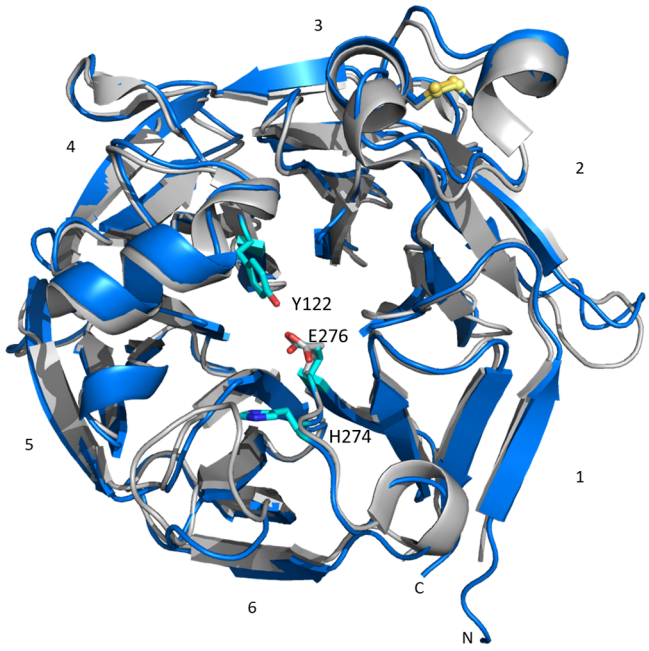

Figure 1. Overlay of structures of *Op*STR (blue) and *Rs*STR (gray, PDB 2v91). Residues mentioned in this paper are highlighted in cyan. Ligands are not displayed.

connected by a conserved disulfide bridge formed between residues Cys60 and Cys72 in *Op*STR (numbering of residues is adapted to the amino acid sequence devoid of a N-terminal signal peptide that is removed for improved expression[20b]).

Soaking experiments with apo-crystals of *Op*STR with THBCs were unsuccessful. However, *Op*STR readily cocrystallized in the presence of racemic THBCs *rac*-**3a–c** and yielded diffracting crystals with the corresponding ligand coordinated in the active site pocket. In the observed orientation of ligand **3** in the active site, the aliphatic substituent of the THBCs (isobutyl for **3a**) points into the active site pocket; thus, the *β*-carboline is pointing outside. This is in contrast to the structures of STR from *Rauvolfia serpentina* with the natural product (*S*)-strictosidine (PDB code: 2v91), where the *β*-carboline points into the active site pocket and the aldehyde side chain protrudes from the active site. Despite the switched orientation of the molecule, the position of the nitrogen atom of the indole moiety of the ligands (*S*)-strictosidine and **3a** is similar and in close proximity to the active site glutamate residue (Glu309 in *Rs*STR, Glu276 in *Op*STR; Figure 2A). All ligands found in crystal structures determined from cocrystallization experiments with racemic THBCs (**3a–c**) adopted a similar orientation in the active site (Figure 2B). The distances from the N atom to Glu276 found in the crystal structures range between 2.8 Å (structure with **3b**) and 3.6 Å (structure with **3c**). The most surprising finding however was that in all cases exclusively the (*S*)-enantiomers of **3a–c** were identified in the active site of *Op*STR, which represents the opposite enantiomer of the preferred (*R*)-product formed in the corresponding enzymatic reactions. However, no crystals were formed when using optically pure (*R*)-**3a**, which is produced by the enzyme with >98% ee, as ligand for cocrystallization,

Because the obtained crystal structures contained the (*S*)- and not the expected (*R*)-enantiomers, it was suspected that the (*S*)-THBC may act as inhibitor, due to the higher affinity

https://dx.doi.org/10.1021/jacs.9b08704
J. Am. Chem. Soc. 2020, 142, 792−800

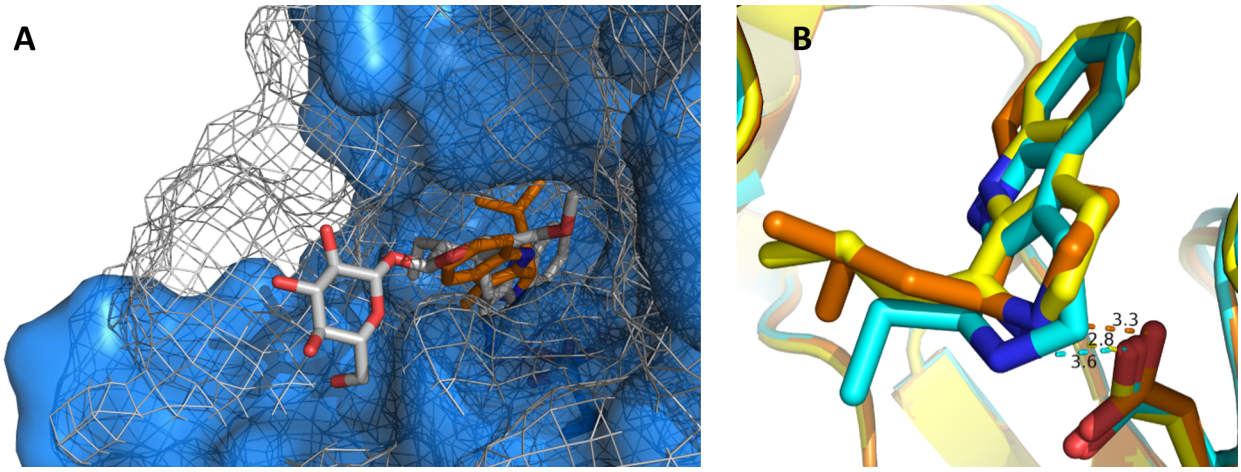

Figure 2. *Op*STR and *Rs*STR with THBCs as ligands. (A) Comparison of *Op*STR (blue) containing **3a** (orange) with *Rs*STR (gray mesh) containing (*S*)-strictosidine (gray, PDB: 2V91). (B) Alignment of different THBC ligands coordinated in *Op*STR. The active site glutamate Glu276 coordinating the N atom is displayed as stick representation. The ligands are depicted in the following colors: **3a**, orange; **3b**, yellow; **3c**, cyan.

of this enantiomer to the enzyme. Indeed, when testing the *Op*STR in a reaction between **1** and **2a** adding (*S*)-, (*R*)-, or *rac*-**3d**, the IC_{50} values calculated from experimentally determined reaction rates indicate that **3d** has inhibitory effects on *Op*STR (Table 1).

Table 1. Summary of IC_{50} Values Determined from Curve Fits of Experimentally Determined Values (determined from Figures S4−S6, Supporting Information)[a]

compound	IC_{50} [mM]
rac-**3d**	3.4 ± 0.3
(*S*)-**3d**	1.6 ± 0.1
(*R*)-**3d**	n.a.

[a]Reactions were run with 10 mM tryptamine **1**, 50 mM isovaleraldehyde **3a** in PIPES (500 μL, 50 mM, pH 7.0, 10% v/v DMSO) in the presence of **3d** (0.01−20 mM) catalyzed by 100 μg of purified *Op*STR (~5.5 μM) at 35 °C, 650 rpm. Velocities were determined by following the formation of product for 3 h. Normalized reaction rates were plotted in a semilogarithmic plot using the SigmaPlot Standard Curves Analysis macro to determine the IC_{50} values. n.a.: not applicable.

While the (*S*)-enantiomer (*S*)-**3d** led to inhibition of the reaction already at low concentration, the mirror image (*R*)-**3d** led to inhibition only at higher concentrations. Thus, product inhibition is mainly caused by the (*S*)-enantiomer. On the basis of this observation, we concluded that the crystal structures obtained most likely did not show the product ligand in a catalytically productive conformation but rather revealed the inhibition of the enzyme by (*S*)-THBCs.

Despite the acquisition of the *Op*STR structures, the ligand complexes did not provide information on the binding mode of (*R*)-THBCs and thus did not explain the observed stereopreference. To gain more insight into the basis for selective transformation by *Op*STR, a stable amine mimic **4** of the imine intermediate **int-I** formed from tryptamine and isobutyraldehyde **2a** was designed (Figure 3). In the structure of *Op*STR obtained by cocrystallization with **4**, two ligand molecules were found in each protein monomer. The active site was occupied by one ligand, while another ligand was bound to the periphery of the enzyme (Figure 3). In the peripheral site, the amine nitrogen was approximately 3.0 Å from the side chain of Glu6, but mutation of this residue to alanine gave a mutant with activity comparable to the wild type, suggesting that this is not a secondary active site. In contrast, the Glu276Ala variant was not active, showing that this is the residue responsible for activity. In the active site, the aliphatic side chain of **4** was pointing into the active site pocket, while the indole moiety

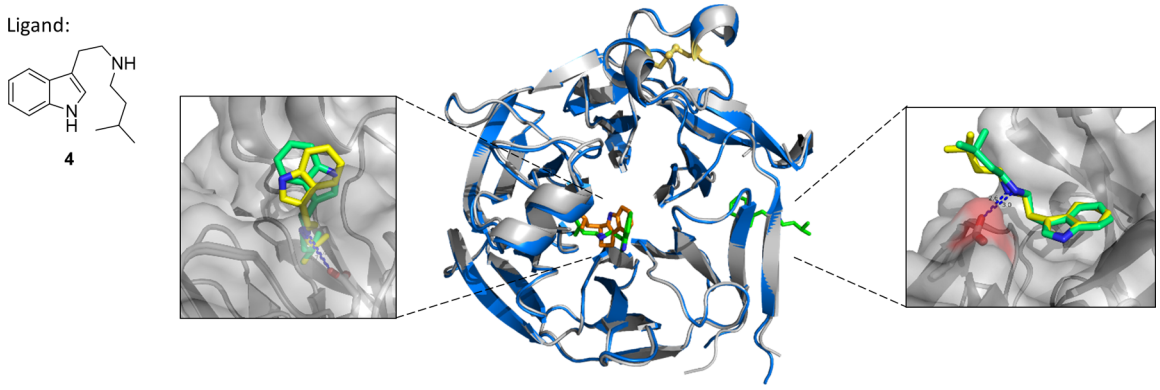

Figure 3. *Op*STR cocrystallized with amine **4** as ligand. The figure shows a comparison between *Op*STR with amine **4** (green) bound (displayed in blue) and *Op*STR with THBC **3a** (protein depicted in gray, ligand in orange). Furthermore, the orientations of **4** found in the active site of *Op*STR and in the outer coordination site at Glu6 are displayed.

https://dx.doi.org/10.1021/jacs.9b08704
J. Am. Chem. Soc. 2020, 142, 792−800

was pointing toward the enzyme surface, in different orientations in each monomer dictated by rotation around the side chain, suggestive of the mobility required to achieve proximity to the imine bond for ring closure in a reactive complex. The alicyclic nitrogen atom is located at a distance of 4.2−4.7 Å from the side chain of Glu279, in approximately the same location as the endocyclic nitrogen of (*S*)-**3a**, with the isobutyl group again held in a hydrophobic pocket formed by Phe197, Trp120, and Tyr122, in a similar mode to that seen in (*S*)-**3a**.

To investigate the influence of these active site residues including the essential Glu276 on the reaction, variants were generated (Table S5). The exchange of Glu276 to aspartate yielded an active variant; however, the stereoselectivity in reactions between **1** and **2a** or **2d** dropped significantly from >98% ee and 76% ee to 92% and 8%, respectively. The same effect was observed for variants of Trp120 with sterically less demanding residues such as alanine, phenylalanine, and tyrosine and for Tyr122Phe. Variant Tyr122Leu was not active. Actually, also products with lower ee were obtained for the variants Phe197Tyr/Trp/Leu. Thus, the variants generated indicate that all these active side residues contribute to the high stereoselectivity observed by the wild type enzyme for the transformation of isovaleraldehyde **2a** with **1**, but they do not give a hint for the switch of stereopreference compared to the reaction of secologanin with **1**.

To better understand the switch of stereopreference, a combined density functional theory (DFT) and molecular dynamics (MD) study was undertaken. The Pictet−Spengler reaction follows a well-studied mechanism,[3,17c,d,20a,21] and we computed the free energy barrier for the analogue to confirm the rate-determining step (Figure 4) at the M06-2X/6-311+

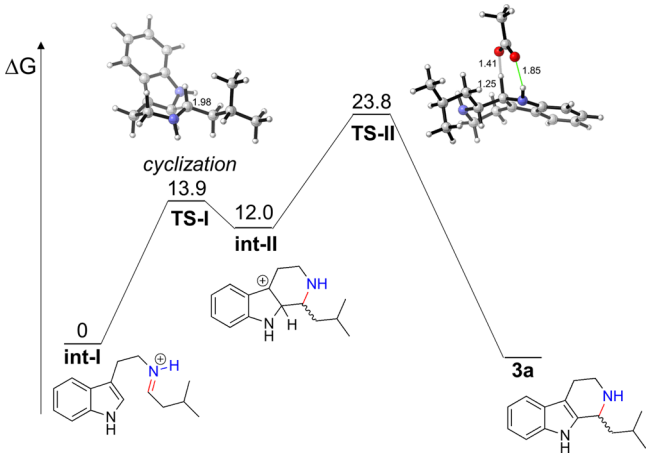

Figure 4. Free energy profile of the Pictet−Spengler reaction between tryptamine (**1**) and **2a** calculated at the M06-2X/6-311++G(2d,2p)-SMD // M06-2X/6-31+G(d,p)-SMD level of theory. Distances are in angstroms (Å). Energies are shown in kcal/mol.

+G(2d,2p)-SMD // M06-2X/6-31+G(d,p)-SMD level of theory with the water solvation model. All intermediates and transition structures were computed from exhaustive conformational searches, and the lowest-energy conformations are shown in Figure 4. In agreement with previous computational studies,[9b] we found the cyclization barrier from iminium **int-I** to be low and reversible ($\Delta G^{\ddagger}$ = 13.9 kcal/mol), leading to the carbocation intermediate **int-II**. This is consistent with the structural data that showed the mobility of the indole in the binding site. We modeled the deprotonation and rearomatization step with a free acetate molecule to simulate the catalytic glutamate residue. The deprotonation transition structure **TS-II** has a barrier of 23.8 kcal/mol, leading directly to the product **3a**. It is well-known that the deprotonation step is rate-determining, while the cyclization establishes the stereochemistry of the new stereogenic center. Based on these results, and previous studies, the cyclization step is reversible, and the enzyme deprotonates only one of the stereoisomeric intermediates to form the product. We chose to model the carbocation intermediate **int-II** for both the analogue and strictosidine in molecular dynamics simulations to determine which stereoisomeric intermediate is able to acquire the best near-attack-conformation for deprotonation.[22]

To understand first the stereopreference of the STR for the natural strictosidine substrate, we performed molecular dynamics simulations on the carbocation intermediate **int-II** for (*S*)- and (*R*)-strictosidine. The intermediates were docked into the binding pocket with Autodock Vina,[23] and the best-scoring pose was selected as the input for 500 ns of MD simulations using Amber.[24] The purpose of the MD simulations was to determine which stereoisomeric intermediate is stable in the binding pocket and best resembles the near-attack-conformation for deprotonation. In principle, the intermediate with the optimal near-attack-conformation between the hydrogen (of the carbocation) and the catalytic glutamate residue would be predicted to have a lower energy barrier for rearomatization.

Snapshots for (*S*)- and (*R*)-strictosidine-int, the analogous carbocation intermediates of **int-II** for strictosidine, are shown in Figure 5. Figure 5A illustrates a snapshot of the carbocation (*S*)-strictosidine-int in the protein pocket. The interaction between the glutamate oxygen and hydrogen for deprotonation is shown in blue dashed lines. The catalytic triad (tyrosine, glutamate, and histidine) as well as residues that interact strongly with the glucose side chain of strictosidine are shown. Figure 5B shows a snapshot of the carbocation (*R*)-strictosidine-int in the protein pocket. The interaction between the glutamate oxygen and hydrogen for deprotonation is shown in red dashed lines. Similarly, only the catalytic triad and residues interacting with strictosidine are shown for clarity.

The distance between the hydrogen H_A and the oxygens on the catalytic glutamate were monitored throughout the MD simulation, which is plotted in Figure 5C. For the (*S*)-strictosidine-int carbocation, the trajectory showed that conformations are sampled for roughly 150 ns until a highly stable conformation is located at 175 ns, which remains for the 500 ns simulation. This is shown for one trajectory in Figure 5C by the blue line. These results are found in triplicate MD simulations. The (*R*)-strictosidine-int carbocation, by contrast, is unable to find a stable conformation in the binding pocket and adopts a binding pose to the surface of the protein. The red line in Figure 5C shows the H···O distance and illustrates how the intermediate changes conformations roughly every 50 ns until the 150 ns region where the intermediate exits from the binding pocket. These results are found in triplicate, unless a different starting geometry is used for (*R*)-strictosidine-int where the hydrogen for deprotonation is on the opposite face of the indole ring.

In these MD simulations, the polar interactions between the residues in Figure 5A and 5B with the strictosidine glucose unit were observed. For the (*S*)-intermediate, the interactions are maintained throughout the 500 ns of the MD simulation. In

https://dx.doi.org/10.1021/jacs.9b08704
J. Am. Chem. Soc. 2020, 142, 792−800

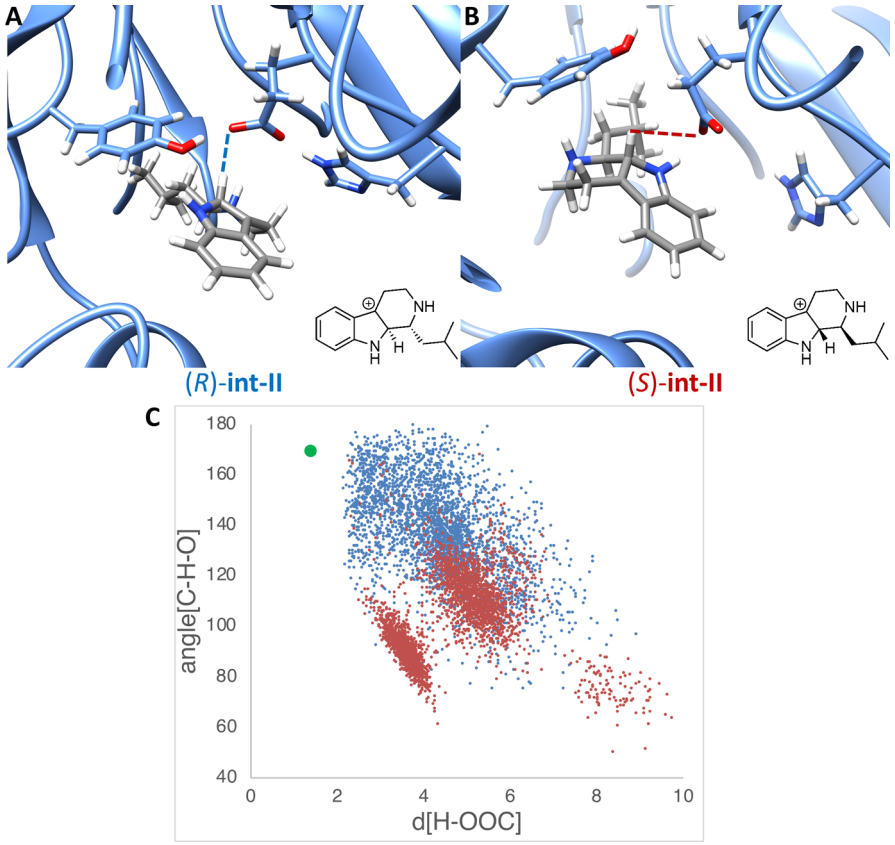

Figure 5. Results from MD simulation with (*S*)- and (*R*)-strictosidine-int. (A) Snapshot of MD trajectory of (*S*)-strictosidine-int. (B) Snapshot of MD trajectory of (*R*)-strictosidine-int. (C) Plot of hydrogen (of (*R*/*S*)-strictosidine-int) to oxygen (of glutamate) distances vs time in nanoseconds throughout the MD trajectory. The blue line represents the distance for (*S*)-strictosidine-int and the red line represents the distance for (*R*)-strictosidine-int.

contrast, the (*R*) intermediate cannot accommodate those interactions while being in a near-attack-conformation for H_A and the glutamate oxygen. When the carbocation is flipped, a stable conformation is found with proximal polar interactions in the MD simulation, but deprotonation cannot occur from this geometry. Thus, we can extrapolate that the strictosidine synthase shows the known stereopreference because the polar glucose unit anchors the substrate into the binding pocket by binding to a specific region of the protein surface. This conformation places the tryptamine unit of the carbocation tightly in the hydrophobic region of the binding pocket. The observed stereoisomer, (*S*)-strictosidine, forms because a near-attack-conformation is highly preferred. The alternative stereoisomer is not formed because there are insufficient stabilizing interactions for the (*R*)-strictosidine intermediate around the binding pocket to anchor the substrate to the catalytic residue, and consequently the deprotonation is very slow.

While the stereospecificity of strictosidine was established with MD simulations, we continued to investigate why the stereoselectivity switches with small aliphatic aldehydes such as isovaleraldehyde **2a**. We performed MD simulations on the stereoisomers of the analogue substrate carbocations **int-II**. Snapshots for each 500 ns MD simulation [(*R*)- and (*S*)-**int-II**] are shown in Figure 6A and 6B. In both MD simulations, the isobutyl substituent on the chiral center prefers to bind on the inside of the binding pocket, in contrast to strictosidine which prefers tryptamine in the binding pocket. In each snapshot, only the catalytic triad is shown. During the 500 ns trajectories, stable conformations are found for both stereoisomers within close distances to the catalytic glutamate.

However, the trajectories differ for the stereoisomeric intermediates at the near-attack-conformation geometry. In snapshot A, the (*R*)-**int-II** H−O distance is proximal, and the catalytic triad is conserved with close interactions. However, (*S*)-**int-II**, shown in snapshot B, the catalytic triad fails to form a strong hydrogen bond consistently for a majority of the 500 ns trajectory. This occurs for a majority of the 500 ns trajectory. The glutamate, while proximal to the substrate, develops a C−H−O angle between 60° and 120° throughout the MD simulation. Few snapshots reach the near-attack-conformation and a geometry near the quantum chemical transition structure for the (*S*)-analogue. The distances between the hydrogen of the carbocations and the oxygen of the glutamates were plotted against the C−H−O angle, which are both required parameters for the deprotonation, shown in Figure 6C. The green data point represents the ideal transition structure optimized with density functional theory in Figure 4. The data in Figure 6C show a clear trend in which (*R*)-**int-II** often achieves a conformation close to the transition structure, or an optimal near-attack-conformation, whereas (*S*)-**int-II** has a poor geometry for deprotonation despite being proximal to the catalytic residue. The difference in geometry between (*R*)-**int-II** and (*S*)-**int-II** is the location of the isobutyl group. In (*R*)-**int-II**, the isobutyl group moves into the area that is occupied by the tryptamine core in strictosidine, whereas in (*S*)-**int-II** the isobutyl group adopts a position close to the backbone of the protein and interferes sterically with the

https://dx.doi.org/10.1021/jacs.9b08704
J. Am. Chem. Soc. 2020, 142, 792−800

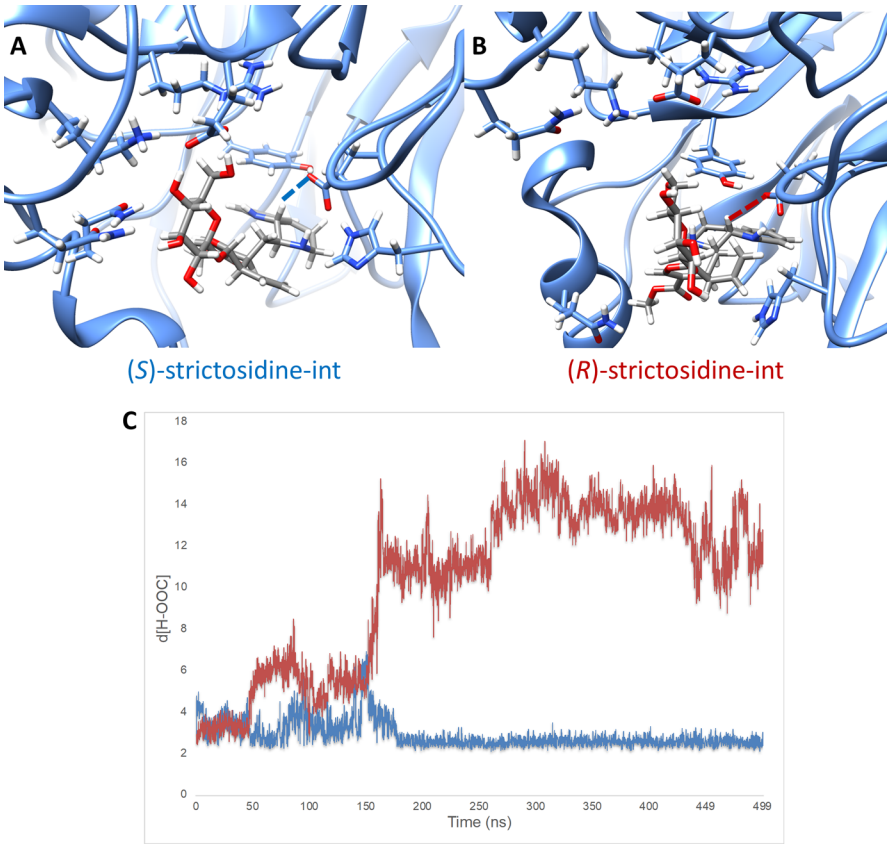

Figure 6. Results from MD simulation with (*R*)- and (*S*)-**int-II**. (A) Snapshot of MD trajectory of (*R*)-**int-II**. (B) Snapshot of MD trajectory of (*S*)-**int-II**. (C) Plot of hydrogen (of **int-II**) to oxygen (of glutamate) distances vs C−H−O angles throughout the MD trajectory, with the transition state geometry shown in green. The blue data points are results from the MD trajectory with (*R*)-**int-II**, and the red data points are results from the MD trajectory with (*S*)-**int-II**.

glutamate residue, similar to that observed for the inhibiting enantiomer in the X-ray complex with (*S*)-**3a** as well as for amine **4**. This illustrates the switch in stereopreference, as well as the lack of stereospecificity with the smaller aldehydes. Because both stereoisomers can reach a near-attack-conformation with a stable geometry, both stereoisomers are formed but (*R*)-**int-II** is preferred.

Due to the suggested changed binding mode of tryptamine **1** in the reaction with **2a** compared to the natural reaction with secologanin, the K_M for tryptamine **1** was determined in the reaction between **1** and **2a** and found to be 1.24 ± 0.13 mM. This value is just about twice the value reported for the K_M of tryptamine **1** with secologanin (0.5 mM) for *Op*STR.[25] Literature values for the K_M for the natural substrate secologanin vary between 3.9×10^{-2} mM[17c] and 4 mM[18e] for STR wild types, while the here determined K_M for the non-natural substrate isovaleraldehyde **2a** is slightly higher at 5.36 ± 0.83 mM.

It is also worth to mention that Glu276 is the active residue in the active site in the natural reaction (tryptamine with secologanin) as well as in the here-described inverted binding mode. This was demonstrated by the exchange of Glu276 to alanine, which resulted in an inactive protein.

CONCLUSIONS

In the (organo)catalytic Pictet−Spengler reaction investigated, the stereochemistry-determining reaction involves the deprotonation of the (*S*)- and (*R*)-intermediates. The MD simulations indicate clearly a binding mode of the natural intermediate and the substrate in which the indole part is pointing to the periphery of the enzyme, a conformation that was also observed for the inhibiting enantiomer in the X-ray complex with (*S*)-**3a** as well as for amine **4** mimicking the iminium **int-II**. By contrast, the alkyl group of the aldehyde, not bound by hydrogen binding present for secologanin, dominates binding with unnatural aldehydes. Thus, it can be concluded that the observed switch in stereopreference is due to a switch of positioning of the reacting substrate parts compared to the natural reaction of tryptamine with secologanin. Remarkably, the same catalyst can have two different productive binding modes for one substrate, here tryptamine, which lead finally to opposite absolute configurations of the product. Furthermore, as tryptamine serves as one reaction partner for both reactions, the one with the natural substrate secologanin as well as the reaction with isovaleraldehyde, the binding mode seems to be controlled by the aldehyde and not the tryptamine part. Furthermore, the investigations revealed that the minor enantiomer formed in the reaction may act as an inhibitor. These insights have profound significance for the future engineering of STRs to ensure on the one hand that the amino acids in the appropriate region are addressed for tuning the catalyst and on the other hand to consider that the minor enantiomer is either not formed or cannot bind. STRs thus present an unusual set of considerations for the engineering of enzyme activity that may have relevance to other systems where enzymes are required to transform substrates very different from those accepted in the native reaction.

https://dx.doi.org/10.1021/jacs.9b08704
J. Am. Chem. Soc. 2020, 142, 792−800

■ ASSOCIATED CONTENT

Supporting Information

The Supporting Information is available free of charge at https://pubs.acs.org/doi/10.1021/jacs.9b08704.

Detailed experimental procedures and information on crystallographic data collection, structure refinement, and MD simulations (PDF)

■ AUTHOR INFORMATION

Corresponding Authors

Gideon Grogan − *University of York, Heslington, U.K.;* orcid.org/0000-0003-1383-7056; Email: gideon.grogan@york.ac.uk

K. N. Houk − *University of California, Los Angeles, California;* orcid.org/0000-0002-8387-5261; Email: houk@chem.ucla.edu

Wolfgang Kroutil − *University of Graz, Graz, Austria;* orcid.org/0000-0002-2151-6394; Email: wolfgang.kroutil@uni-graz.at

Other Authors

Elisabeth Eger − *University of Graz, Graz, Austria*

Adam Simon − *University of California, Los Angeles, California;* orcid.org/0000-0001-6334-3359

Mahima Sharma − *University of York, Heslington, U.K.;* orcid.org/0000-0003-3960-2212

Song Yang − *University of California, Los Angeles, California*

Willem B. Breukelaar − *University of Graz, Graz, Austria*

Complete contact information is available at: https://pubs.acs.org/10.1021/jacs.9b08704

Author Contributions

All authors have given approval to the final version of the manuscript.

Notes

The authors declare no competing financial interest.

■ ACKNOWLEDGMENTS

The research leading to these results was funded partly by the Austrian Science Fund (FWF, project W9-01, DK Molecular Enzymology). M.S. was funded by grant BB/M006832/1 from the UK Biotechnology and Biological Sciences Research Council. We thank Dr. Johan P. Turkenburg and Mr. Sam Hart for assistance with X-ray data collection, and the Diamond Light Source for access to beamline I04-1 under proposal number mx-9948. We are grateful to the National Institutes of General Medical Sciences, National Institutes of Health, for research grant GM-124480 to K.N.H., and Chemistry-Biology Interface Research Training Grant (T32GM008496) for a traineeship to A.S. Computational resources from the UCLA Institute of Digital Research and Education (IDRE) are gratefully acknowledged.

■ REFERENCES

(1) Khan, A. Y.; Suresh Kumar, G. Natural isoquinoline alkaloids: binding aspects to functional proteins, serum albumins, hemoglobin, and lysozyme. *Biophys. Rev.* **2015**, *7*, 407−420.

(2) Cao, R.; Peng, W.; Wang, Z.; Xu, A. β-Carboline Alkaloids: Biochemical and Pharmacological Functions. *Curr. Med. Chem.* **2007**, *14*, 479−500.

(3) Pictet, A.; Spengler, T. Über die Bildung von Isochinolin-derivaten durch Einwirkung von Methylal auf Phenyl-äthylamin, Phenyl-alanin und Tyrosin. *Ber. Dtsch. Chem. Ges.* **1911**, *44*, 2030−2036.

(4) (a) Cox, E. D.; Hamaker, L. K.; Li, J.; Yu, P.; Czerwinski, K. M.; Deng, L.; Bennett, D. W.; Cook, J. M.; Watson, W. H.; Krawiec, M. Enantiospecific formation of trans 1,3-Disubstituted Tetrahydro-β-carbolines by the Pictet−Spengler reaction and Conversion of Cis Diastereomers into their trans counterparts by Scission of the C-1/N-2 Bond. *J. Org. Chem.* **1997**, *62*, 44−61. (b) Bailey, P. D.; Moore, M. H.; Morgan, K. M.; Smith, D. I.; Vernon, J. M. Enhancing the yield and diastereoselectivity of the Pictet−Spengler reaction: A highly efficient route to Cis-1,3-disubstituted tetrahydro-β-carbolines. *Tetrahedron Lett.* **1994**, *35*, 3587−3588. (c) Alberch, L.; et al. The cis-Specific Pictet−Spengler Reaction. *Eur. J. Org. Chem.* **2004**, *2004*, 1887−1890. (d) Bailey, P. D.; Beard, M. A.; Phillips, T. R. Unexpected cis selectivity in the Pictet−Spengler reaction. *Tetrahedron Lett.* **2009**, *50*, 3645−3647.

(5) Ducrot, P.; Rabhi, C.; Thal, C. Synthesis of tetrahydro-β-carbolines and studies of the pictet−spengler reaction. *Tetrahedron* **2000**, *56*, 2683−2692.

(6) (a) Kawate, T.; Yamanaka, M.; Nakagawa, M. Chiral auxiliary approach to the asymmetric Pictet−Spengler reaction of tryptamines. *Heterocycles* **1999**, *50*, 1033−1039. (b) Soe, T.; Kawate, T.; Fukui, N.; Nakagawa, M. Asymmetric Pictet−Spengler reaction with chiral-N-(β-3-indoly) ethyl-1-methylbenzylamine. *Tetrahedron Lett.* **1995**, *36*, 1857−1860. (c) Gremmen, C.; Willemse, B.; Wanner, M. J.; Koomen, G.-J. Enantiopure Tetrahydro-β-carbolines via Pictet−Spengler Reactions with N-Sulfinyl Tryptamines. *Org. Lett.* **2000**, *2*, 1955−1958. (d) Waldmann, H.; Schmidt, G.; Henke, H.; Burkard, M. Asymmetric Pictet−Spengler reactions employing N,N-phthaloyl amino acids as chiral auxiliary groups. *Angew. Chem., Int. Ed. Engl.* **1995**, *34*, 2402−2403.

(7) (a) Seayad, J.; Seayad, A. M.; List, B. Catalytic Asymmetric Pictet−Spengler Reaction. *J. Am. Chem. Soc.* **2006**, *128*, 1086−1087. (b) Wanner, M. J.; van der Haas, R. N.; de Cuba, K. R.; van Maarseveen, J. H.; Hiemstra, H. Catalytic asymmetric Pictet−Spengler reactions via sulfenyliminium ions. *Angew. Chem., Int. Ed.* **2007**, *46*, 7485−7487. (c) Sewgobind, N. V.; Wanner, M. J.; Ingemann, S.; de Gelder, R.; van Maarseveen, J. H.; Hiemstra, H. Enantioselective Binol-phosphoric acid catalyzed Pictet−Spengler reactions of N-benzyltryptamine. *J. Org. Chem.* **2008**, *73*, 6405−6408. (d) Muratore, M. E.; Holloway, C. A.; Pilling, A. W.; Storer, R. I.; Trevitt, G.; Dixon, D. J. Enantioselective Brønsted acid-catalyzed N-acyliminium cyclization cascades. *J. Am. Chem. Soc.* **2009**, *131*, 10796−10797. (e) Holloway, C. A.; Muratore, M. E.; Storer, R. l.; Dixon, D. J. Direct Enantioselective Brønsted Acid Catalyzed N-Acyliminium Cyclization Cascades of Tryptamines and Ketoacids. *Org. Lett.* **2010**, *12*, 4720−4723. (f) Wang, S. G.; Xia, Z. L.; Xu, R. Q.; Liu, X. J.; Zheng, C.; You, S. L. Construction of Chiral Tetrahydro-β-Carbolines: Asymmetric Pictet−Spengler Reaction of Indolyl Dihydropyridines. *Angew. Chem., Int. Ed.* **2017**, *56*, 7440−7443.

(8) (a) Ishihara, K.; Miyata, M.; Hattori, K.; Tada, T.; Yamamoto, H. A new chiral BLA promoter for asymmetric aza Diels-Alder and Aldol-type reactions of imines. *J. Am. Chem. Soc.* **1994**, *116*, 10520−10524. (b) Yamada, H.; Kawate, T.; Matsumizu, M.; Nishida, A.; Yamaguchi, K.; Nakagawa, M. Chiral Lewis Acid-Mediated Enantioselective Pictet−Spengler Reaction of N b-Hydroxytryptamine with Aldehydes. *J. Org. Chem.* **1998**, *63*, 6348−6354. (c) Bou-Hamdan, F. R.; Leighton, J. L. Highly Enantioselective Pictet−Spengler Reactions with α-Ketoamide-Derived Ketimines: Access to an Unusual Class of Quaternary α-Amino Amides. *Angew. Chem., Int. Ed.* **2009**, *48*, 2403−2406.

(9) (a) Taylor, M. S.; Jacobsen, E. N. Highly enantioselective catalytic acyl-Pictet−Spengler reactions. *J. Am. Chem. Soc.* **2004**, *126*, 10558−10559. (b) Klausen, R. S.; Kennedy, C. R.; Hyde, A. M.;

Jacobsen, E. N. Chiral Thioureas Promote Enantioselective Pictet−Spengler Cyclization by Stabilizing Every Intermediate and Transition State in the Carboxylic Acid-Catalyzed Reaction. *J. Am. Chem. Soc.* **2017**, *139*, 12299−12309. (c) Raheem, I. T.; Thiara, P. S.; Peterson, E. A.; Jacobsen, E. N. Enantioselective Pictet−Spengler-type cyclizations of hydroxylactams: H-bond donor catalysis by anion binding. *J. Am. Chem. Soc.* **2007**, *129*, 13404−13405. (d) Mergott, D. J.; Zuend, S. J.; Jacobsen, E. N. Catalytic asymmetric total synthesis of (+)-yohimbine. *Org. Lett.* **2008**, *10*, 745−748.

(10) Stockigt, J.; Zenk, M. H. Strictosidine (isovincoside): the key intermediate in the biosynthesis of monoterpenoid indole alkaloids. *J. Chem. Soc., Chem. Commun.* **1977**, 646−648.

(11) (a) Rueffer, M.; El-Shagi, H.; Nagakura, N.; Zenk, M. H. (S)-norlaudanosoline synthase: The first enzyme in the benzylisoquinoline biosynthetic pathway. *FEBS Lett.* **1981**, *129*, 5−9. (b) Samanani, N.; Facchini, P. J. Purification and Characterization of Norcoclaurine Synthase: the First Committed Enzyme in Benzylisoquinoline Alkaloid Biosynthesis in Plants. *J. Biol. Chem.* **2002**, *277*, 33878−33883. (c) Luk, L. Y. P.; Bunn, S.; Liscombe, D. K.; Facchini, P. J.; Tanner, M. E. Mechanistic Studies on Norcoclaurine Synthase of Benzylisoquinoline Alkaloid Biosynthesis: An Enzymatic Pictet−Spengler Reaction. *Biochemistry* **2007**, *46*, 10153−10161. (d) Ilari, A.; Franceschini, S.; Bonamore, A.; Arenghi, F.; Botta, B.; Macone, A.; Pasquo, A.; Bellucci, L.; Boffi, A. Structural Basis of Enzymatic (*S*)-Norcoclaurine Biosynthesis. *J. Biol. Chem.* **2009**, *284*, 897−904. (e) Lichman, B. R.; Gershater, M. C.; Lamming, E. D.; Pesnot, T.; Sula, A.; Keep, N. H.; Hailes, H. C.; Ward, J. M. 'Dopamine-first' mechanism enables the rational engineering of the norcoclaurine synthase aldehyde activity profile. *FEBS J.* **2015**, *282*, 1137−1151. (f) Pesnot, T.; Gershater, M. C.; Ward, J. M.; Hailes, H. C. The Catalytic Potential of Coptis japonica NCS2 Revealed − Development and Utilisation of a Fluorescamine-Based Assay. *Adv. Synth. Catal.* **2012**, *354*, 2997−3008. (g) Lechner, H.; Soriano, P.; Poschner, R.; Hailes, H. C.; Ward, J. M.; Kroutil, W. Library of Norcoclaurine Synthases and Their Immobilization for Biocatalytic Transformations. *Biotechnol. J.* **2018**, *13*, 1700542.

(12) (a) De-Eknamkul, W.; Ounaroon, A.; Tanahashi, T.; Kutchan, T. M.; Zenk, M. H. Enzymatic condensation of dopamine and secologanin by cell-free extracts of Alangium lamarckii. *Phytochemistry* **1997**, *45*, 477−484. (b) De-Eknamkul, W.; Suttipanta, N.; Kutchan, T. M. Purification and characterization of deacetylipecoside synthase from Alangium lamarckii Thw. *Phytochemistry* **2000**, *55*, 177−181.

(13) (a) Koketsu, K.; Minami, A.; Watanabe, K.; Oguri, H.; Oikawa, H. Pictet−Spenglerase involved in tetrahydroisoquinoline antibiotic biosynthesis. *Curr. Opin. Chem. Biol.* **2012**, *16*, 142−149. (b) Koketsu, K.; Watanabe, K.; Suda, H.; Oguri, H.; Oikawa, H. Reconstruction of the saframycin core scaffold defines dual Pictet−Spengler mechanisms. *Nat. Chem. Biol.* **2010**, *6*, 408.

(14) (a) Mori, T.; Hoshino, S.; Sahashi, S.; Wakimoto, T.; Matsui, T.; Morita, H.; Abe, I. Structural Basis for *β*-Carboline Alkaloid Production by the Microbial Homodimeric Enzyme McbB. *Chem. Biol.* **2015**, *22*, 898−906. (b) Chen, Q.; Ji, C.; Song, Y.; Huang, H.; Ma, J.; Tian, X.; Ju, J. Discovery of McbB, an Enzyme Catalyzing the *β*-Carboline Skeleton Construction in the Marinacarboline Biosynthetic Pathway. *Angew. Chem., Int. Ed.* **2013**, *52*, 9980−9984.

(15) Chen, Q.; Zhang, S.; Xie, Y. Characterization of a new microbial Pictet−Spenglerase NscbB affording the *β*-carboline skeletons from Nocardiopsis synnemataformans DSM 44143. *J. Biotechnol.* **2018**, *281*, 137−143.

(16) Brown, R. T.; Leonard, J.; Sleigh, S. K. The role of strictosidine in monoterpenoid indole alkaloid biosynthesis. *Phytochemistry* **1978**, *17*, 899−900.

(17) (a) Ma, X.; Koepke, J.; Fritzsch, G.; Diem, R.; Kutchan, T. M.; Michel, H.; Stöckigt, J. Crystallization and preliminary X-ray crystallographic analysis of strictosidine synthase from Rauvolfia: the first member of a novel enzyme family. *Biochim. Biophys. Acta, Proteins Proteomics* **2004**, *1702*, 121−124. (b) Koepke, J.; Ma, X.; Fritzsch, G.; Michel, H.; Stockigt, J. Crystallization and preliminary X-ray analysis of strictosidine synthase and its complex with the substrate tryptamine. *Acta Crystallogr., Sect. D: Biol. Crystallogr.* **2005**, *61*, 690−693. (c) Ma, X.; Panjikar, S.; Koepke, J.; Loris, E.; Stöckigt, J. The Structure of *Rauvolfia serpentina* Strictosidine Synthase Is a Novel Six-Bladed *β*-Propeller Fold in Plant Proteins. *Plant Cell* **2006**, *18*, 907−920. (d) Maresh, J. J.; Giddings, L.-A.; Friedrich, A.; Loris, E. A.; Panjikar, S.; Trout, B. L.; Stöckigt, J.; Peters, B.; O'Connor, S. E. Strictosidine synthase: Mechanism of a Pictet−spengler catalyzing enzyme. *J. Am. Chem. Soc.* **2008**, *130*, 710−723. (e) Stöckigt, J.; Barleben, L.; Panjikar, S.; Loris, E. A. 3D-Structure and function of strictosidine synthase − the key enzyme of monoterpenoid indole alkaloid biosynthesis. *Plant Physiol. Biochem.* **2008**, *46*, 340−355.

(18) (a) Bernhardt, P.; McCoy, E.; O'Connor, S. E. Rapid Identification of Enzyme Variants for Reengineered Alkaloid Biosynthesis in Periwinkle. *Chem. Biol.* **2007**, *14*, 888−897. (b) Yamazaki, M.; Asano, T.; Yamazaki, Y.; Sirikantaramas, S.; Sudo, H.; Saito, K. Biosynthetic system of camptothecin: an anticancer plant product. *Pure Appl. Chem.* **2010**, *82*, 213−218. (c) McCoy, E.; Galan, M. C.; O'Connor, S. E. Substrate specificity of strictosidine synthase. *Bioorg. Med. Chem. Lett.* **2006**, *16*, 2475−2478. (d) Loris, E. A.; Panjikar, S.; Ruppert, M.; Barleben, L.; Unger, M.; Schübel, H.; Stöckigt, J. Structure-Based Engineering of Strictosidine Synthase: Auxiliary for Alkaloid Libraries. *Chem. Biol.* **2007**, *14*, 979−985. (e) Hampp, N.; Zenk, M. H. Homogeneous strictosidine synthase from cell suspension cultures of Rauvolfia serpentina. *Phytochemistry* **1988**, *27*, 3811−3815. (f) Wu, F.; Zhu, H.; Sun, L.; Rajendran, C.; Wang, M.; Ren, X.; Panjikar, S.; Cherkasov, A.; Zou, H.; Stöckigt, J. Scaffold tailoring by a newly detected Pictet−Spenglerase activity of strictosidine synthase: from the common tryptoline skeleton to the rare piperazino-indole framework. *J. Am. Chem. Soc.* **2012**, *134*, 1498−1500. (g) Yang, L.; Zou, H.; Zhu, H.; Ruppert, M.; Gong, J.; Stöckigt, J. Improved Expression of His6-Tagged Strictosidine Synthase cDNA for Chemo-Enzymatic Alkaloid Diversification. *Chem. Biodiversity* **2010**, *7*, 860−870.

(19) (a) Treimer, J. F.; Zenk, M. H. Purification and Properties of Strictosidine Synthase, the Key Enzyme in Indole Alkaloid Formation. *Eur. J. Biochem.* **1979**, *101*, 225−233. (b) Chen, S.; Galan, M. C.; Coltharp, C.; O'Connor, S. E. Redesign of a Central Enzyme in Alkaloid Biosynthesis. *Chem. Biol.* **2006**, *13*, 1137−1141.

(20) (a) Bernhardt, P.; Usera, A. R.; O'Connor, S. E. Biocatalytic asymmetric formation of tetrahydro-*β*-carbolines. *Tetrahedron Lett.* **2010**, *51*, 4400−4402. (b) Pressnitz, D.; Fischereder, E.-M.; Pletz, J.; Kofler, C.; Hammerer, L.; Hiebler, K.; Lechner, H.; Richter, N.; Eger, E.; Kroutil, W. Asymmetric Synthesis of (*R*)-1-Alkyl-Substituted Tetrahydro-ß-carbolines Catalyzed by Strictosidine Synthases. *Angew. Chem., Int. Ed.* **2018**, *57*, 10683−10687.

(21) (a) Ungemach, F.; Cook, J. M. The Spiroindolenine Intermediate. A Review. *Heterocycles* **1978**, *9*, 1089−1119. (b) Bailey, P. Direct proof of the involvement of a spiro intermediate in the Pictet−Spengler reaction. *J. Chem. Res., Synop* **1987**, 202−203.

(22) Hur, S.; Bruice, T. C. The near attack conformation approach to the study of the chorismate to prephenate reaction. *Proc. Natl. Acad. Sci. U. S. A.* **2003**, *100*, 12015−12020.

(23) Trott, O.; Olson, A. J. AutoDock Vina: Improving the speed and accuracy of docking with a new scoring function, efficient optimization, and multithreading. *J. Comput. Chem.* **2010**, *31*, 455−461.

(24) Case, D. A.; Ben-Shalom, I. Y.; Brozell, S. R.; Cerutti, D. S.; Cheatham, T. E., III; Cruzeiro, V. W. D.; Darden, T. A.; Duke, R. E.; Ghoreishi, D.; Gilson, M. K.; Gohlke, H.; Goetz, A. W.; Greene, D.; Harris, R.; Homeyer, N.; Izadi, S; Kovalenko, A.; Kurtzman, T.; Lee, T. S.; LeGrand, S.; Li, P.; Lin, S.; Liu, J.; Luchko, T.; Luo, R.; Mermelstein, D. J.; Merz, K. M.; Miao, Y.; Monard, G.; Nguyen, C.; Nguyen, H.; Omelyan, I.; Onufriev, A.; Pan, F; Qi, R.; Roe, D. R.; Roitberg, A.; Sagui, C.; Schott-Verdugo, S.; Shen, J.; Simmerling, C. L.; Smith, J.; Salomon-Ferrer, R.; Swails, J.; Walker, R. C.; Wang, J.; Wei, H.; Wolf, R. M.; Wu, X.; Xiao, L.; York, D. M.; Kollman, P. A. *AMBER 2018*, University of California: San Francisco, 2018.

(25) Yamazaki, Y.; Urano, A.; Sudo, H.; Kitajima, M.; Takayama, H.; Yamazaki, M.; Aimi, N.; Saito, K. Metabolite profiling of alkaloids and

https://dx.doi.org/10.1021/jacs.9b08704
J. Am. Chem. Soc. 2020, 142, 792−800

strictosidine synthase activity in camptothecin producing plants. *Phytochemistry* **2003**, *62*, 461−470.

https://dx.doi.org/10.1021/jacs.9b08704
J. Am. Chem. Soc. 2020, 142, 792−800